Journal of Alloys and Compounds 509 (2011) 6158–6162

Contents lists available at ScienceDirect

Journal of Alloys and Compounds

journal homepage: www.elsevier.com/locate/jallcom

Microwave synthesis, structure, and magnetic properties of quasi-one-dimensional complex oxide $Sr_4LiMn_2O_9$

G.V. Bazuev*, A.P. Tyutyunnik, I.F. Berger, I.V. Nikolaenko, B.G. Golovkin

Institute of Solid State Chemistry, Ural Branch of the Russian Academy of Sciences, 620990 Ekaterinburg, GSP, Russia

ARTICLE INFO

Article history:
Received 24 November 2010
Received in revised form 17 February 2011
Accepted 5 March 2011
Available online 12 March 2011

Keywords:
Quasi-one-dimensional oxides
Synthesis
Crystal structures
Magnetic properties

ABSTRACT

The complex oxide $Sr_4LiMn_2O_9$ belonging to the $A_{3n+3m}A'_nMn_{3m+n}O_{9m+6n}$ family ($m=3, n=1$) was prepared from a mixture of $SrCO_3$ and $LiMn_2O_4$ in a microwave furnace by the solid state reaction. The results of structural refinements and magnetic properties are presented. The crystal structure of $Sr_4LiMn_2O_9$ was solved using simultaneously X-ray and neutron diffraction data with the GSAS program in the space group *P*321 with unit cell parameters: $a=9.5721(7)$ Å, $c=7.8264(5)$ Å, $V=621.025$ Å^3, $Z=3$. $Sr_4LiMn_2O_9$ was found to contain 2 independent 1D chains of face-shared polyhedrons with a sequence of two octahedrons and one trigonal prism. The chains are separated by strontium cations. The refinement results show that the octahedrons and trigonal prisms in the first chain orderly contain Mn and Li, respectively, whereas the second chain is characterized by mixed occupation of these structural positions. The temperature dependence of the magnetic susceptibility of $Sr_4LiMn_2O_9$ was found to be due to antiferromagnetically coupled dimers from magnetic Mn cations.

1. Introduction

In the last decade, the family of complex oxides with the composition $A_{3n+3m}A'_nMn_{3m+n}O_{9m+6n}$, where A – Ca, Sr, Ba; A′ – 3d-elements, Mg, and Na [1,2], was added to the numerous groups of manganese oxide compounds. The oxides of this family are structurally similar to hexagonal compounds 2H $BaMnO_3$ and Sr_4PtO_6 and contain parallel chains stretching along the *c* axis. The chains consist of face-shared octahedrons MnO_6 and trigonal prisms $A'O_6$. The crystal structure of these compounds features high isolation of chains from each other, which is due to A^{2+} cations located in distorted square antiprisms. Such structure dictates highly anisotropic physical, in particular, magnetic properties of these compounds, which can be used as model objects for studying one-dimensional (1D) electronic behavior. Depending on the positions and electronic configurations of the transition metals, the compounds can form a 1D or three-dimensional magnetic order or exhibit magnetic frustration. So, much interest was aroused recently by the discovery of collinear-magnetic-driven ferroelectricity in a diatomic Ising chain of Ca_3CoMnO_6 [3], which belongs to the considered family at $m=0$, $n=1$ [4].

The ratio between the number of octahedrons and trigonal prisms in the chains is different for compounds with different compositions, and this determines the peculiarities of their structure and properties. To date, more than 10 groups of complex oxides belonging to the $A_{3n+3m}A'_nMn_{3m+n}O_{9m+6n}$ family [2] have been obtained including $A_3A'MnO_6$, $A_4A'Mn_2O_9$, $A_5A'MnO_{12}$, $A_6A'Mn_4O_{15}$, $A_9A'_2Mn_5O_{21}$, $A_{14}A'_3Mn_8O_{33}$, and some others. The majority of these compounds are formed on the basis of bivalent cations of alkaline earth and 3d elements and tetravalent manganese. Meanwhile, analogous compounds based on platinum group elements (Pt, Ir, Ru, Rh) are represented by a much wider variety of cationic combinations. So, platinoids in $A_3A'BO_6$ oxides can be in tri- (Rh), tetra- (Rh, Pt, Ir, Ru), and pentavalent (Ru, Ir, Rh) states.

Synthesis of $Ba_4NaMn_2O_9$, which has a quasi-1D structure with parameters $a=10.006(2)$ Å, $c=8.210(3)$ Å (space group *P*321) and belongs to the $A_{3n+3m}A'_nB_{3m+n}O_{9m+6n}$ ($n=3$, $m=1$) family, was reported in [5,6]. This compound was synthesized electrochemically as single crystals in NaOH melt. Attempts to synthesize this compound from $BaCO_3/Ba(OH)_2{\cdot}3H_2O$, MnO_2/Mn_2O_3, and Na_2CO_3 using the solid-state reaction in different experiment conditions (during heating in air, in nitrogen or NaOH flux flow) failed. The authors [5] believe that $Ba_4NaMn_2O_9$ is the first compound containing manganese in the form of cations with the average oxidation state +4.5. The structural studies showed that trigonal-prismatic positions in $Ba_4NaMn_2O_9$ are occupied by Na^+ cations, whereas manganese is in octahedral positions. Note that in this work neither magnetic nor spectroscopic studies confirmed the presence of different-valence manganese cations. No evidence was obtained of an ordered arrangement of Mn^{4+} and Mn^{5+} cations in structural positions.

A similar hexagonal phase was also registered in the Sr–Li–Mn–O system, which is formed during solid-phase synthe-

* Corresponding author. Tel.: +7 343 374 4943; fax: +7 343 374 4495.
E-mail address: bazuev@ihim.uran.ru (G.V. Bazuev).

0925-8388/$ – see front matter © 2011 Elsevier B.V. All rights reserved.
doi:10.1016/j.jallcom.2011.03.040

sis from manganese oxide and lithium and strontium carbonates [7]. The X-ray diffraction pattern of this phase (nominal composition Sr_3LiMnO_x) was satisfactorily indexed (like $Sr_4Ni_3O_9$ [8] and $Sr_{12}Ni_{7.5}O_{27}$ [9]) in the space group *P*321 with parameters $a = 9.42(1)$ and $c = 7.85(1)$ Å. However, the formula $Sr_4LiMn_2O_9$ could not be attributed to this phase since in addition to the above hexagonal phase the impurity compound $Sr_7Mn_4O_{15}$ [10] was always formed in the samples during solid-phase synthesis.

In this work we report the formation condition, the results of structural studies, as well as the magnetic properties for the complex oxide $Sr_4LiMn_2O_9$.

2. Experimental

$SrCO_3$, Li_2CO_3 and MnO_2 were used as initial reagents for the synthesis of $Sr_4LiMn_2O_9$ by means of the solid-phase reaction. At first, the complex oxide $LiMn_2O_4$ was obtained from MnO_2 and Li_2CO_3 at 800 °C in air. Then $LiMn_2O_4$ reacted with the strontium carbonate $SrCO_3$ at 950–1000 °C in air to produce the final product. The samples were reground after 15 and 30 h of annealing. The total heat treatment time was 48 h.

In the second technique of $Sr_4LiMn_2O_9$ synthesis, microwave absorption was used for the reaction between the mentioned initial components. The main advantages in the application of microwave heating in chemical processes are due to the peculiarities of microwave energy absorption by a substance. There is no need to waste the energy for heating of the furnace or reactor walls. In contrast to other commonly used methods, microwaves permit volumetric heating of materials, which considerably reduces the time and temperature of solid-phase transformations. In this work we used a SVCh-laborant microwave muffle furnace produced by NPO Ural-Gefest with the nominal capacity of the SHF generator 700 W and frequency 2450 MHz. The furnace is equipped with heating rods, which heat up to the required temperature by absorbing the electromagnetic energy. A chromel–alumel thermocouple located in the space between the rods was used for temperature control. The thermocouple has a cover made of non-corrosive steel, which protects against electromagnetic field.

The purity of the synthesized product was checked using X-ray powder diffraction (XRD) patterns collected at room temperature on a STADI P (STOE) diffractometer in transmission geometry with a linear mini-PSD detector using Cu$K\alpha_1$ radiation in the 2θ range from 2 to 120° with a step of 0.02°. Polycrystalline silicon ($a = 5.43075(5)$ Å) was used as an external standard. Neutron diffraction data were collected from 5 to 120° 2θ with a step of 0.1° and neutron wavelength $\lambda = 1.531$ Å using a D2A setup of the reactor IVV 2M (Zarechny, Russia). Possible impurity phases were checked by comparing their XRD patterns with those in the PDF2 database (ICDD, USA, Release 2009).

The crystal structure of $Sr_4LiMn_2O_9$ was refined simultaneously with X-ray and neutron powder diffraction data using the GSAS software [11]. The peak profiles were fitted with a pseudo-Voigt function $I(2\theta) = x \times L(2\theta) + (1-x) \times G(2\theta)$ (where *L* and *G* are the Lorentzian and Gaussian part, respectively). The angular dependence of the peak width was described by the relation $(FWHM)^2 = Utg^2\theta + Vtg\theta + W$, where *FWHM* is the full line width at half maximum. The background level was described by a combination of thirty-six-order Chebyshev polynomials. The absorption correction function for a flat plate sample in transmission geometry was applied [11].

The magnetic measurements were carried out on an MPMS-5-XL SQUID magnetometer produced by QUANTUM DESIGN. A 0.2 g sintered sample was placed into a gelatin capsule. The temperature was varied in the interval from 2 to 300 or to 400 K. The applied magnetic field was 0.5 and 5 kOe. Temperature dependences of magnetization *M* and magnetic susceptibility χ were determined for two experiment modes: ZFC and FC. In the ZFC mode, the sample was cooled to the temperature 2 K, then magnetic field of a given intensity $H = \text{const}$ was applied, and magnetization was measured during heating. In the FC mode, when a high final temperature was reached, the sample was cooled in the magnetic field of the same intensity, and measurements were taken during cooling. Magnetization *M* and static magnetic susceptibility $\chi = M/H$ were determined from the measurements of the static magnetic moment of the sample. The dynamic magnetic susceptibility measurement technique was used to determine the real χ' and imaginary χ'' components of magnetic susceptibility for the amplitude value of alternating magnetic field to 4 Oe at frequency 80 Hz.

3. Results and discussion

3.1. Synthesis and structural characterization

As was noted in [7], in the attempt to synthesize $Sr_4LiMn_2O_4$ from $SrCO_3$, Li_2CO_3, and MnO_2 under usual condition at 950–1000 °C, the resulted product contained $Sr_7Mn_4O_{15}$ along with a hexagonal $Sr_4Ni_3O_9$-type phase. Chemical analysis showed that

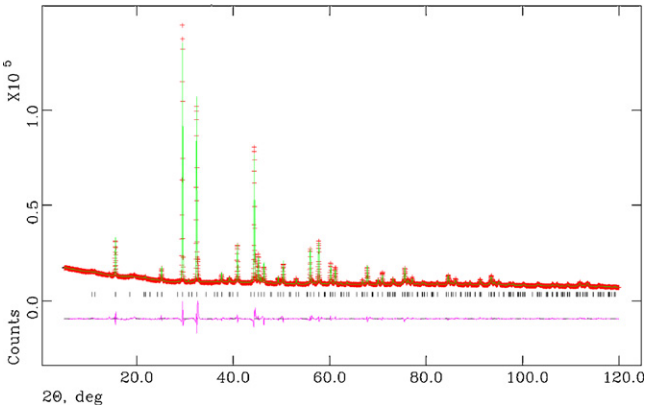

Fig. 1. Observed (crosses), calculated (solid line), and difference (bottom line) X-ray powder diffraction patterns of $Sr_4LiMn_2O_9$.

the content of lithium in the as-synthesized samples was much smaller than the nominal content for $Sr_4LiMn_2O_9$. The low lithium content was due to the evaporation of Li_2O formed during decomposition of Li_2CO_3 at high temperatures. Therefore, in this work we used $LiMn_2O_4$ as the initial substance, which had been preliminarily obtained from Li_2CO_3 and MnO_2 at 800 °C in air. According to [12], this oxide decomposes to $LiMnO_2$, Mn_3O_4, and O_2 at 900 °C, $LiMnO_2$ being stable in air at 1000 °C and above. Thus, using this compound as a precursor, we hoped to eliminate the loss of lithium during synthesis.

Synthesis according to reaction

$$4SrCO_3 + LiMn_2O_4 = Sr_4LiMn_2O_9 + 4CO_2$$

at temperature 950–1000 °C in air for 48 h led to the formation of a product, whose X-ray diffraction pattern is satisfactorily described in the space group *P*321 with the parameters close to those reported in [7]. However, this technique also failed to produce a sample free of the impurity manganate $Sr_7Mn_4O_{15}$. The pure Sr_4LiMnO_9 was synthesized in a microwave furnace. A mixture of initial reagents $SrCO_3$ and $LiMn_2O_4$ in the amount of 4 g was preliminarily calcined at 950 °C for 1 h. Then the product was ground, pressed at pressure 3000 kg/cm^2, and annealed at 1030 °C for 2 h with intermediate grinding after 1 h of annealing.

The sample of $Sr_4LiMn_2O_9$ obtained as a result of microwave treatment at 1030 °C was a deep-brown crystalline powder. According to the energy dispersion spectroscopy data, the Sr/Mn ratio in the examined sample particles was found to be 1.92, i.e. close to 2.

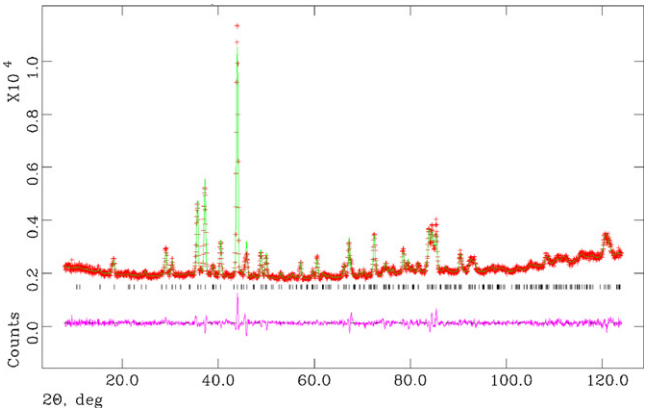

Fig. 2. Observed (circles), calculated (solid line), and difference (bottom line) neutron powder diffraction patterns of $Sr_4LiMn_2O_9$.

Table 1
Atomic coordinates and isotropic thermal parameters ($U_{iso} \times 100$, Å^2) for $Sr_4LiMn_2O_9$.

Atom		x/a	y/b	z/c	Fraction	$U_{iso} \times 100^2$
Sr(1)	6g	0.025(2)	0.691(1)	0.244(1)	1.0	2.1(1)
Sr(2)	3f	0.324(2)	0.0	0.5	1.0	2.1(1)
Sr(3)	3e	0.359(2)	0.0	0.0	1.0	2.1(1)
Li	1a	0.0	0.0	0.0	1.0	2.1(1)
Mn	2c	0.0	0.0	0.326(3)	1.0	2.1(1)
Mn/Li(1)	2d	1/3	2/3	0.106(5)	0.86/0.14(3)	2.1(1)
Mn/Li(2)	2d	1/3	2/3	0.422(5)	0.80/0.20(4)	2.1(1)
Mn/Li(3)	2d	1/3	2/3	0.793(4)	0.50/0.50(2)	2.1(1)
O(1)	6g	0.813(5)	0.495(5)	0.028(4)	1.0	2.1(1)
O(2)	6g	0.165(4)	0.014(4)	0.188(3)	1.0	2.1(1)
O(3)	6g	0.170(4)	0.518(6)	0.271(4)	1.0	2.1(1)
O(4)	6g	0.678(4)	0.187(4)	0.452(4)	1.0	2.1(1)
O(5)	3f	0.844(7)	0.0	0.5	1.0	2.1(1)

X-ray: wRp = 4.06%, Rp = 2.19%, $R(F^2) = 6.19\%$.
Neutrons: wRp = 3.58%, Rp = 2.70%, $R(F^2) = 7.21\%$.

Figs. 1 and 2 display experimental, theoretical, and difference X-ray and neutron powder diffraction patterns for a sample of $Sr_4LiMn_2O_9$, respectively. The results of crystal structure refinement listed in Table 1 confirm that the complex oxide $Sr_4LiMn_2O_9$ is isostructural with $Sr_4AMn_2O_9$ (A = Cu [13,14], Co [15], Zn, Mg [14,16]) and $Ba_4NaMn_2O_9$ [5] and belongs to the family of 2H-hexagonal perovskites $A_{3n+3m}A'_nMn_{3m+n}O_{9m+6n}$ at $m = 1$ and $n = 3$. The trigonal cell parameters in the space group $P321$ (No. 150) are $a = 9.5721(7)$ Å, $c = 7.8264(5)$ Å, $V = 621.025$ Å^3. It is interesting that unit cell parameters of $Sr_4LiMn_2O_9$ are almost similar to those for $Sr_4AMn_2O_9$ (A = Cu, Zn, Ni) although the radius of Li^+ is greater than that of A^{2+} [17]. Table 2 gives the main cation–anion interatomic distances. Fig. 3 demonstrates a model crystal structure of $Sr_4LiMn_2O_9$ corresponding to the refined atomic coordinates (Table 1). A distinctive feature of this structure is the presence of chains, which consist of edge-shared octahedrons and tetragonal prisms and are parallel to the c axis. The chains are separated by Sr^{2+} cations located in 8-, 9- and 10-fold oxygen polyhedrons. As follows from Table 1 and Fig. 3, two types of chains with different compositions can be distinguished. In the A chain, the octahedrons are occupied by manganese (2c positions), while the trigonal prisms (1a positions) – by lithium. The octahedral environment in this case is represented by oxygen anions O2 and O5. The B chain consists of octahedrons with Mn/Li1 and Mn/Li2 and trigonal prisms with Mn/Li3. In this case, cations are coordinated with oxygen anions O1, O3, and O4.

As a rule, octahedrons in such compounds are occupied by cations having smaller ionic radii, while trigonal prisms host cations with larger radii. Taking into account the considerable difference in ionic radii of Li^{1+} (0.76 Å) and Mn^{4+}/Mn^{5+} (0.53/0.33 Å) [17], we think it is natural that the trigonal-prismatic positions (1a) in the A chain are completely occupied by lithium, whereas the octahedral positions (2c) – by manganese. The mixed occupancy of octahedral and trigonal-prismatic positions in the B chain should be considered apparently as the necessary condition for the stabilization of the crystal structure of this complex oxide. A similar mixed state was also observed in other compounds of this family. So, in [18] it was established by neutron diffraction refinements that nickel in trigonal prisms in Ca_3NiMnO_6 is partially replaced by manganese, and the chemical composition corresponds to $Ca_3Ni_{0.92}Mn_{1.08}O_3$. Magnetic susceptibility measurements and Mn-K-edge XANES spectra [19] showed that 10% of Mn and Zn in $Sr_4ZnMn_2O_9$ exchange their positions in 1D chains.

The actual composition of the oxide – $Sr_4Li_{0.89}Mn_{2.11}O_9$ – was determined from atomic positions occupancies (Table 1). The Sr/Mn ratio for this composition is 1.90, which is close to that established in energy-dispersion analysis (1.92). Note that the deviation of the chemical composition of $Sr_4LiMn_2O_9$ from the ideal stoichiometric composition is not an exception. So, the formulas $Sr_4Cu_{0.91}Mn_{2.09}O_9$ [20] and $Sr_4Zn_{0.95}Mn_{2.05}O_9$ [14] were derived by refinement of the parameters and the distribution of cations in structural positions.

It should be taken into account that the error in determination of metal–oxygen bond lengths (Table 2) is large enough because of a rather high structural disorder. The average Mn–O distance in the first chain (1.94 Å) is within the typical values for Mn^{4+} cations in octahedral oxide positions [5,14,21]. The presence of Li^+ cations in the octahedral positions of the second chain results in a decrease

Table 2
Interatomic distances d (Å) for $Sr_4LiMn_2O_9$.

Sr(1)–O(1)	2.59(4)	Sr(2)–O(2)	2.92(3)	Sr(3)–O(1)	2.65(5)
Sr(1)–O(1)	2.66(4)	Sr(2)–O(2)	2.92(3)	Sr(3)–O(1)	2.70(5)
Sr(1)–O(2)	2.72(4)	Sr(2)–O(3)	2.50(4)	Sr(3)–O(1)	2.70(5)
Sr(1)–O(2)	2.69(4)	Sr(2)–O(3)	2.50(4)	Sr(3)–O(1)	2.65(5)
Sr(1)–O(3)	2.65(5)	Sr(2)–O(4)	2.96(4)	Sr(3)–O(2)	2.42(4)
Sr(1)–O(3)	2.70(5)	Sr(2)–O(4)	2.71(3)	Sr(3)–O(2)	2.42(4)
Sr(1)–O(4)	2.56(3)	Sr(2)–O(4)	2.71(3)	Sr(3)–O(3)	2.64(4)
Sr(1)–O(4)	2.88(3)	Sr(2)–O(4)	2.96(4)	Sr(3)–O(3)	2.64(4)
Sr(1)–O(4)	2.56(4)	Sr(2)–O(5)	2.69(2)		
		Sr(2)–O(5)	2.69(2)		
Average	2.67	Average	2.74	Average	2.60
Mn/Li(1)–O(1)	3 × 1.81(4)	Mn/Li(2)–O(3)	3 × 1.91(4)	Mn/Li(3)–O(1)	3 × 2.04(4)
Mn/Li(1)–O(3)	3 × 1.98(4)	Mn/Li(2)–O(4)	3 × 1.76(4)	Mn/Li(3)–O(4)	3 × 2.41(4)
Average	1.90	Average	1.835	Average	2.225
Mn–O(2)	3 × 1.86(4)	Li–O(2)	6 × 2.12(3)		
Mn–O(5)	3 × 2.02(5)				
Average	1.94	Average	2.12		
Mn–Mn	2.55				
Mn/Li(1)–Mn(Li2)	2.47				

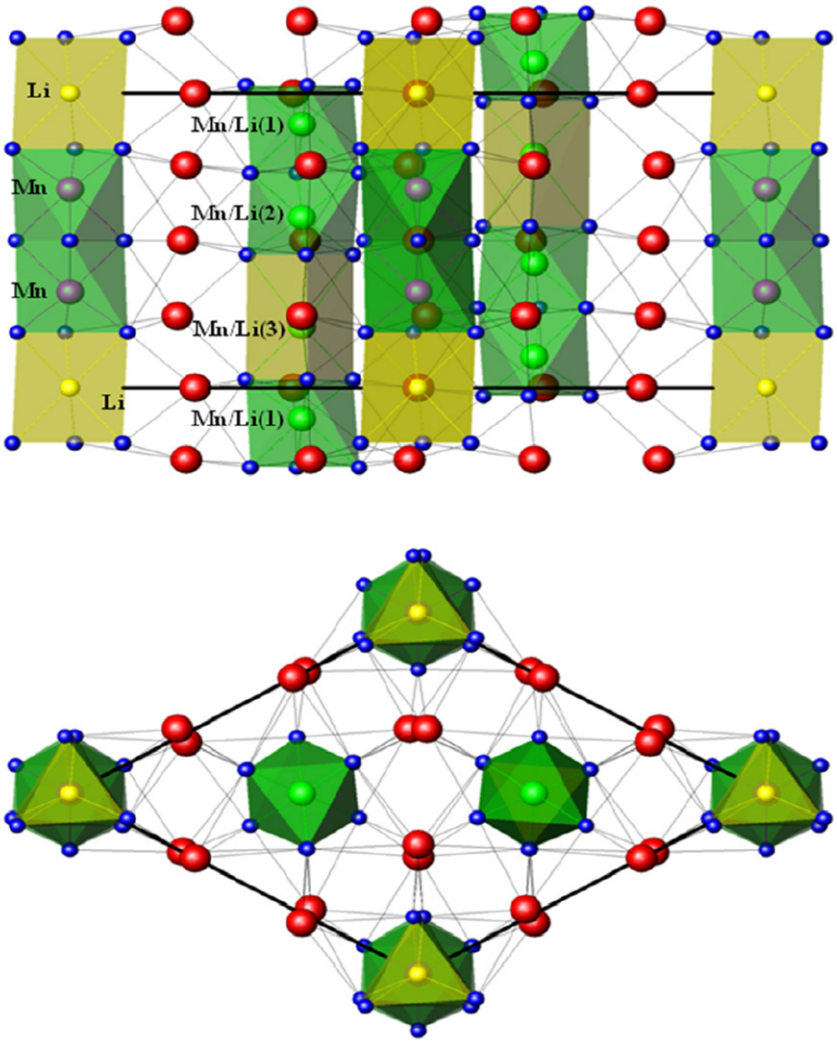

Fig. 3. Crystal structure of $Sr_4LiMn_2O_9$. Light (yellow) polyhedrons are trigonal prisms, shaded (green) polyhedrons are octahedrons. Filled (red) circles represent Sr cations in the inter-chain space. (For interpretation of the references to color in this figure legend, the reader is referred to the web version of the article.)

in the Mn/Li1–O1 and Mn/Li2–O1 bond lengths to the average values 1.90 and 1.83 Å, respectively. The average Li–O distance in the *A* chain is 2.12(3) Å, which is somewhat smaller than the typical bond lengths (2.21–2.26 Å) in A_3LiBO_6 compounds (A = Sr, Ca; B = Ir, Ru [22]), but is close to the typical bond lengths (2.035–2.152 Å) in octahedral positions of Ln_2LiIrO_6 perovskites (Ln = La, Pr, Nd, Sm, Eu) [23]. Average Mn/Li(3)–O distances in the trigonal prism of the *B* chain (2.22 Å) are even larger than the Li–O bond length in the *A* chain in spite of the fact that 50% of Mn cations occupy this position.

The average oxidation state of manganese in $Sr_4Li_{0.89}Mn_{2.11}O_9$ is +4.32. However, no reliable conclusion can be made about the presence of Mn^{5+} cations or higher degrees of oxidation of this element on the basis of structural analysis. We may only suppose that high-valence Mn cations can occupy octahedral 2d positions of the *B* chain leading to a decrease in the Mn/Li(2)–O(1) bond length to the average value 1.835 Å. It is interesting to note that the two $[LiMn_2O_9]_\infty$ chains differ in their inter-cation distances: the Mn(Li1)–Mn(Li2) distances within dimers of chain *A* are 2.47 Å, while the Mn–Mn distances within dimers of chain *B* are 2.55 Å. Usually, similar compounds exhibit smaller discrepancy between Mn–Mn distances in Mn_2O_9 chain dimers (0.02–0.03 Å in

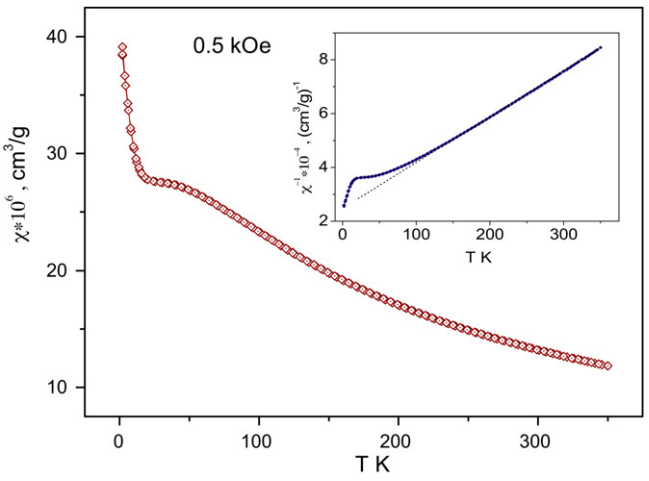

Fig. 4. Temperature dependence of magnetic susceptibility χ for $Sr_4LiMn_2O_9$ (H = 0.5 kOe). The inset shows the $1/\chi = f(T)$dependence.

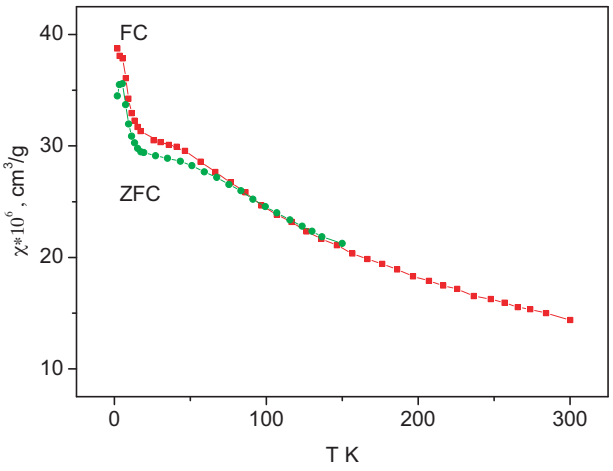

Fig. 5. Temperature dependence of the real part of dynamic magnetic susceptibility χ' for $Sr_4LiMn_2O_9$.

$Sr_4CuMn_2O_9$, $Sr_4ZnMn_2O_4$ [14], and $Sr_4NiMn_2O_9$ [20]). However, note for comparison that in $Ba_4NaMn_2O_9$ [5] and $Sr_4CoMn_2O_9$ [24] the Mn–Mn distances within dimers of two chains are different too (2.53–2.66 Å and 2.41–2.58 Å, respectively).

3.2. Magnetic properties

The results of static and dynamic magnetic susceptibility measurements for $Sr_4LiMn_2O_9$ are given in Figs. 4 and 5, respectively. As follows from the inset in Fig. 4, magnetic susceptibility χ in the temperature range 250–350 K obeys the Curie–Weiss law

$$\chi = \frac{C}{T-\theta},$$

where χ is molar susceptibility, C is the Curie constant (3.636 cm^3 K/mol), and θ is the Weiss temperature (−140.2 K). The experimental value of the effective magnetic moment (μ_{eff}) for $Sr_4Li_{0.89}Mn_{2.11}O_9$ (5.393 μ_B) is smaller than the theoretical moment (5.63 μ_B) calculated in the assumption that all manganese is present as Mn^{4+} cations. If we consider that 31.8% of manganese are in the form of Mn^{5+}cations as follows from the formula $Sr_4Li_{0.89}Mn_{2.11}O_9$, then the magnetic moment should be equal to 5.192 μ_B. The Weiss temperature θ has a negative value, which is indicative of prevailing antiferromagnetic exchange between magnetic moments.

The deviation of the $\chi = f(T)$ dependence from the Curie–Weiss law in the region of low temperatures is due to structural peculiarities of the examined compound, in particular, to the presence of exchange-bound dimers from magnetic cations of Mn, which occupy face-shared octahedrons. This is attested by a broad maximum at about 40 K. An analogous behavior of $\chi = f(T)$ with broad maxima at 100–150 K was observed for compounds $Sr_4AMn_2O_9$ (A = Zn, Mg, Ni, Cu) [13–16]. Their magnetic properties were discussed in the framework of the model of isotropic exchange between exchange-bound dimers from Mn^{4+} cations during weak inter-chain interaction. This model is quite applicable for the description of the $\chi = f(T)$ dependence in $Sr_4Li_{0.89}Mn_{2.11}O_9$. The displacement of the maximum to the low-temperature region for $Sr_4Li_{0.89}Mn_{2.11}O_9$ is likely to be due to noticeable disordering of manganese cations in the structural positions, as well as to the presence of some manganese in the form of Mn^{5+} cations. At temperatures below 25 K, the susceptibility increases abruptly showing that an essential part of Mn is not bound in dimers, but occupies trigonal-prismatic positions.

The results of dynamic magnetic (AC) susceptibility χ' measurements in the temperature intervals 2–300 K in the FC mode and 2–150 K in the ZFC mode are shown in Fig. 5. It is seen that χ' exhibits the same values as DC susceptibility χ and an analogous temperature dependence with a broad maximum at 40 K. However, as follows from Fig. 5, below 80 K the ZFC and FC curves diverge, which may be indicative of magnetic frustration. The singularities on the curves at 4.5 K suggest that a 3D magnetically ordered (evidently antiferromagnetic) state can emerge through inter-chain interactions between Mn cations. The magnetization vs. magnetic field dependence in the range from −50 to 50 kOe at 2 K is characterized by a small hysteresis (not shown). In order to clarify the nature of the observed magnetic transformation at 4.5 K, additional studies are required.

Acknowledgments

This work was supported by a state contract of the Federal Agency of Science and Innovations (No. 02.518.11.7119) and a grant of the Presidium of the Russian Academy of Sciences. The authors are grateful to M.A. Melkozerova for the energy dispersion spectroscopy investigations.

References

[1] K.E. Stitzer, J. Darriet, H.-C. zur Loye, Curr. Opin. Solid State Mater. Sci. 5 (2001) 535.
[2] G.V. Bazuev, Russ. Chem. Rev. 75 (2006) 749.
[3] Y.J. Choi, H.T. Yi, S. Lee, Q. Huang, V. Kiryukhin, S.-W. Cheong, Phys. Rev. Lett. 100 (2008) 047601.
[4] V.G. Zubkov, G.V. Bazuev, A.P. Tyutyunnik, I.F. Berger, J. Solid State Chem. 160 (2001) 293.
[5] E. Quarez, P. Roussel, H. Leligny, A. Bendraoua, O. Mentre, Solid State Sci. 6 (2004) 931.
[6] P. Roussel, O. Perez, E. Quarez, H. Leligny, O. Mentre, Z. Kristallographie 225 (2010) 1.
[7] N.A. Zaitseva, V.N. Krasilnikov, G.V. Bazuev, G.S. Shekhtman, T.I. Chupakhina, Izv. Akad. Nauk. Ser. Fiz. 68 (2004) 731 (in Russian).
[8] F. Abraham, S. Minaud, C. Renard, J. Mater. Chem. 4 (1994) 1763.
[9] M. Strunk, Hk. Muller-Buschbaum, J. Alloys Compd. 209 (1994) 189.
[10] R. Krigel, A. Feltz, L. Walz, A. Simon, H.J. Mattausch, Z. Anorg. Allg. Chem. 617 (1992) 99.
[11] A.C. Larson, R.B. Von Dreele, GSAS LANSCE, MS-H805, Los Alamos National Laboratory, Los Alamos, NM 87545, 1995, p. 21.
[12] Y.-Il. Jang, W.D. Moorehead, Y.-M. Chiang, Solid State Ionics 149 (2002) 201.
[13] G.V. Bazuev, V.N. Krasilnikov, D.G. Kellerman, J. Alloys Compd. 352 (2003) 190.
[14] C.A. Moore, P.D. Battle, J. Solid State Chem. 176 (2003) 88.
[15] A. El Abed, E. Gaudin, J. Darriet, M.-H. Whangbo, J. Solid State Chem. 163 (2002) 513.
[16] G.V. Bazuev, N.A. Zaitseva, V.N. Krasilnikov, D.G. Kellerman, Russ. J. Inorg. Chem. 48 (2003) 219.
[17] R.D. Shannon, Acta Crystallogr. A 32 (1976) 751.
[18] G.V. Bazuev, V.G. Zubkov, I.F. Berger, T.I. Arbuzova, Solid State Sci. 1 (1999) 365.
[19] J. Chaboy, C. Prieto, M. Hernando, M. Parras, J. Gonzalez-Calbet, Phys. Rev. B 74 (2006) 174433.
[20] A. El Abed, E. Gaudin, J. Darriet, Acta Crystallogr. C 58 (2002) 1138.
[21] V.G. Zubkov, A.P. Tyutyunnik, I.F. Berger, V.I. Voronin, G.V. Bazuev, C.A. Moore, P.D. Battle, J. Solid State Chem. 167 (2002) 453.
[22] M.J. Davis, M.D. Smith, K.E. Stitzer, H.-C. zur Loye, J. Alloys Compd. 351 (2003) 95.
[23] S.J. Mugavero III, M.D. Smith, H.-C. zur Loye, J. Solid State Chem. 178 (2005) 200.
[24] K. Boulahya, M. Parras, J.M. Gonzales-Calbet, J.L. Martinez, Chem. Mater. 15 (2003) 3537.